

Single crystal growth and transport properties of narrow-bandgap semiconductor RhP_2

De-Sheng Wu(吴德胜), Ping Zheng(郑萍), and Jian-Lin Luo(雒建林)
Citation: Chin. Phys. B, 2024, 33 (**8**): 088101. DOI: 10.1088/1674-1056/ad4cd5

What follows is a list of articles you may be interested in

Regulation mechanism of catalyst structure on diamond crystal morphology under HPHT process

Ya-Dong Li(李亚东), Yong-Shan Cheng(程永珊), Meng-Jie Su(宿梦洁), Qi-Fu Ran(冉启甫), Chun-Xiao Wang(王春晓), Hong-An Ma(马红安), Chao Fang(房超), Liang-Chao Chen(陈良超)
Chin. Phys. B, 2020, 29 (**7**): 078101. DOI: 10.1088/1674-1056/ab90e8

Growth of high quality Sr_2IrO_4 epitaxial thin films onconductive substrates

Hui Xu(徐珲), Zhangzhang Cui(崔璋璋), Xiaofang Zhai(翟晓芳), Yalin Lu(陆亚林)
Chin. Phys. B, 2019, 28 (**7**): 078102. DOI: 10.1088/1674-1056/28/7/078102

Excellent thermal stability and thermoelectric properties of *Pnma*-phase SnSe in middle temperature aerobic environment

Yu Tang(唐语), Decong Li(李德聪), Zhong Chen(陈钟), Shuping Deng(邓书平), Luqi Sun(孙璐琪), Wenting Liu(刘文婷), Lanxian Shen(申兰先), Shukang Deng(邓书康)
Chin. Phys. B, 2018, 27 (**11**): 118105. DOI: 10.1088/1674-1056/27/11/118105

A-site ordered quadruple perovskite oxides $AA_3'B_4O_{12}$

Youwen Long(龙有文)
Chin. Phys. B, 2016, 25 (**7**): 078108. DOI: 10.1088/1674-1056/25/7/078108

Influence of vacuum degree on growth of Bi_2Te_3 single crystal

Tang Yan-Kun (唐雁坤), Zhao Wen-Juan (赵文娟), Zhu Hua-Qiang (朱化强), Huang Yong-Chao (黄勇潮), Cao Wei-Wei (曹伟伟), Yang Qian (杨倩), Yao Xiao-Yan (姚晓燕), Zhai Ya (翟亚), Dong Shuai (董帅)
Chin. Phys. B, 2015, 24 (**7**): 078101. DOI: 10.1088/1674-1056/24/7/078101

Single crystal growth and transport properties of narrow-bandgap semiconductor RhP_2

De-Sheng Wu(吴德胜)[1,3,†], Ping Zheng(郑萍)[1,2], and Jian-Lin Luo(雒建林)[1,2,‡]

[1] *Beijing National Laboratory for Condensed Matter Physics, Institute of Physics, Chinese Academy of Sciences, Beijing* 100190, *China*
[2] *Songshan Lake Materials Laboratory, Dongguan* 523808, *China*
[3] *Quantum Science Center of Guangdong–Hong Kong–Macao Greater Bay Area (Guangdong), Shenzhen* 518045, *China*

(Received 21 February 2024; revised manuscript received 26 April 2024; accepted manuscript online 17 May 2024)

We report the growth of high-quality single crystals of RhP_2, and systematically study its structure and physical properties by transport, magnetism, and heat capacity measurements. Single-crystal x-ray diffraction reveals that RhP_2 adopts a monoclinic structure with the cell parameters $a = 5.7347(10)$ Å, $b = 5.7804(11)$ Å, and $c = 5.8222(11)$ Å, space group $P2_1/c$ (No. 14). The electrical resistivity $\rho(T)$ measurements indicate that RhP_2 exhibits narrow-bandgap behavior with the activation energies of 223.1 meV and 27.4 meV for two distinct regions, respectively. The temperature-dependent Hall effect measurements show electron domain transport behavior with a low charge carrier concentration. We find that RhP_2 has a high mobility $\mu_e \sim 210$ cm$^2\cdot$V$^{-1}\cdot$s^{-1} with carrier concentrations $n_e \sim 3.3\times10^{18}$ cm^{-3} at 300 K with a narrow-bandgap feature. The high mobility μ_e reaches the maximum of approximately 340 cm$^2\cdot$V$^{-1}\cdot$s^{-1} with carrier concentrations $n_e \sim 2\times10^{18}$ cm^{-3} at 100 K. No magnetic phase transitions are observed from the susceptibility $\chi(T)$ and specific heat $C_p(T)$ measurements of RhP_2. Our results not only provide effective potential as a material platform for studying exotic physical properties and electron band structures but also motivate further exploration of their potential photovoltaic and optoelectronic applications.

Keywords: single crystal growth, narrow band system, electrical transport, high mobilities

PACS: 81.10.–h, 71.28.+d, 72.15.Eb **DOI:** 10.1088/1674-1056/ad4cd5

1. Introduction

Recently, exploring novel quantum materials in transition metal-based compounds with narrow band gaps has become an important research topic in optoelectronics in modern condensed matter physics.[1–4] Narrow-bandgap semiconductor materials are widely used in optoelectronics owing to their excellent light absorption properties. Many narrow-bandgap compounds such as InAs, InSb, InP, and PbSnTe with excellent thermal and electrical properties have been synthesized to systematically study their exotic physical properties in the past decades.[5–10] The possibility of high conductivity, high mobility, unique band structures, and surface properties has made these materials of great interest in the field of quantum materials. For thermoelectric applications, several narrow-gap semiconductors or semimetals in d-electron materials, such as $FeSb_2$, $CoSb_2$, and $RuSb_2$, have been widely studied.[11–14] For example, $FeSb_2$ has been reported to be a narrow-band nearly magnetic or Kondo semiconductor.[13] The thermal power $S(T)$ in $CoSb_2$ can reach 40 μV/K at 300 K, while the thermal power of $RhSb_2$ reaches 140 μV/K.[13–15] On the other hand, $RhSb_2$ single crystals were reported to exhibit an anomalous peak in resistivity at approximately 200 K, which was explained to be induced by the energy gap at the Y_2 point of the electron band structure.[15] Using angle resolved photoemission spectroscopy (ARPES) and density functional theory (DFT) calculations, researchers found weak topological insulator states of a van Hove singularity (VHS) along the (100) direction near the Fermi energy (E_F) in $RhBi_2$.[16]

RhP_2 polycrystals were reported to have an arsenopyrite-marcasite-type structure isostructural to that of $RhSb_2$ decades ago.[17] However, as far as we know, there is no experimental results reported about the physical properties of single crystals RhP_2. For polycrystals, temperature-dependent resistivity exhibits insulating behavior with an energy gap about 1 eV.[17] The magnetic susceptibility of RhP_2 shows diamagnetism.[18,19] However, the low-temperature physical properties of single-crystal RhP_2 have not yet been systematically studied. These aspects motivated us to grow single crystal of RhP_2 and to study their physical properties of RhP_2 single crystals.

In this work, we grow RhP_2 single crystals by Sn flux method for the first time as far as we know, and carry out detailed studies on its structure and basic physical properties including transport properties, heat capacity, and susceptibility. We find that the RhP_2 single crystals exhibit semiconductor behavior with two broad peaks from 300 K to 2 K, which is different from that of $RhSb_2$ but similar to the case of $FeSb_2$.[11,15] The carrier concentrations $n_e \sim 3.3\times10^{18}$ cm^{-3}

†Corresponding author. E-mail: dswu@iphy.ac.cn
‡Corresponding author. E-mail: jlluo@iphy.ac.cn

© 2024 Chinese Physical Society and IOP Publishing Ltd

with a high mobility $\mu_e \sim 210$ cm^2·V^{-1}·s^{-1} at 300 K are obtained by Hall resistivity measurements. RhP_2 shows no apparent phase transition from the magnetic susceptibility and specific heat measurements. By fitting with the formula $C_p/T = \gamma + \beta T^2$, we obtained the electronic specific heat coefficient $\gamma = 0.44$ mJ·mol^{-1}·K^{-2}, which shows a low-density state of electrons neat the Fermion level. Combined with band calculation results, we propose that these two unusual kinks in temperature-dependent resistivity are related to the narrow-bandgap feature of RhP_2 single crystal. Our results not only provide effective potential as a material platform for studying exotic physical properties and electron band structures but also motivate further exploration of their photovoltaic applications.

2. Experiment details

In our experiment, single crystals of RhP_2 were obtained by using the flux method reported previously.[15,20] The starting materials, Rh (99.99%, BDMT, Co. Ltd), P (99.999%, Alfa), and Sn (99.999%, BDMT, Co. Ltd), were mixed in Al_2O_3 capsules and sealed with a 1/4 amount of Ar atom in a silica tube. The entire silica tube was then rapidly heated to 1373 K in a furnace, held at this temperature for two days. Then, it was cooled to low temperature to spin off the flux via centrifugation. Finally, black and shiny single crystals in 1 mm were thus left. The chemical composition of the RhP_2 was confirmed by energy dispersive x-ray spectroscopy (EDS) using a Hitachi S-4800 scanning electron microscope (SEM). A Bruker SMART APEX Ⅱ diffractometer with Mo $K_{\alpha 1}$ radiation ($\lambda = 0.71073$ Å) were used in the x-ray diffraction (XRD) experiments. Using the SHELXL program, the crystal structure data was refined.[21] The magnetic susceptibility χ from 5 K to 300 K was determined using a SQUID-VSM. The specific heat C_p, the resistivity ρ_{xx}, and Hall coefficient data from 2 K to 300 K were measured with a physical property measurement system (PPMS, Quantum Design).

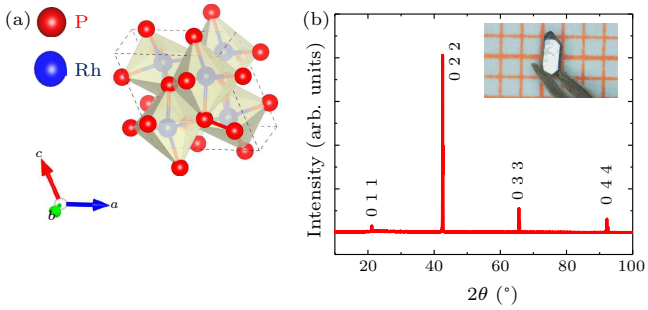


Fig. 1. (a) Crystal structure information of RhP_2. (b) Single crystal XRD data of RhP_2. The inset is an optical picture of typical RhP_2 single crystal used for the x-ray testing.

3. Results and discussion

Similar to the $RhSb_2$ single crystal, RhP_2 in space group $P2_1/c$ belong to the pyrite-marcasite-type structure.[15] Figure 1(b) shows the single-crystal x-ray diffraction data of RhP_2 with the [011] direction. The typical size of RhP_2 single crystal is shown by an optical image in the inset of Fig. 1(b). The EDS results show that the chemical ratios of RhP_2 crystals are 1 : 2 [see Fig. S1 in the supporting information]. The single crystal x-ray refined structure results indicate that RhP_2 single crystals have monoclinic-type structure (space group $P2_1/c$, No. 14). The best structure refinement results show R indices of $R = 0.0585(435)$ and $wR_2 = 0.1547(441)$ using the program SHELXL-2014/7.[22] The lattice parameters $a = 5.7347(10)$ Å, $b = 5.7804(11)$ Å, $c = 5.8222(11)$ Å, $\alpha = \beta = 90°$, and $\gamma = 112.907(6)°$, in accordance with the reported values in polycrystalline samples[17] [see Tables I and Ⅱ in the supporting information].

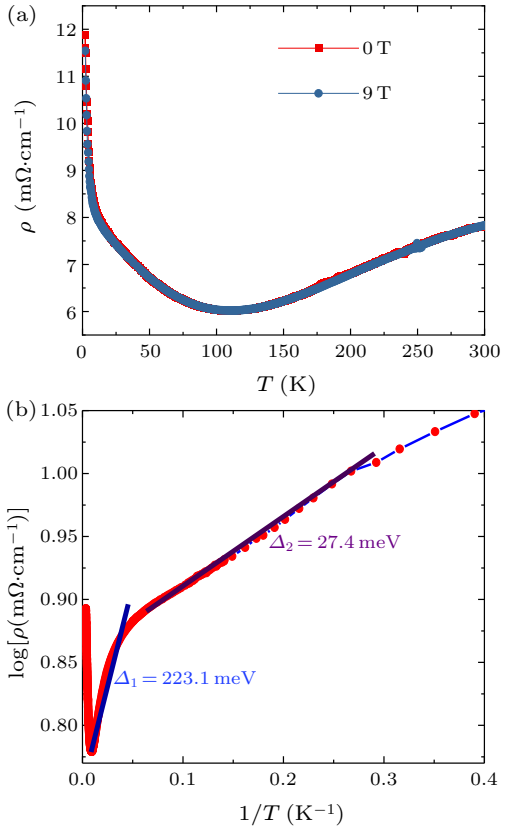


Fig. 2. The transport data of RhP_2 single crystal: (a) the temperature dependence of the resistivity ρ_{xx} of RhP_2 single crystal with an applied magnetic field of 9 T and 0 T, (b) fit data using $\rho(T) = \rho_0 \exp(\Delta/k_B T)$, resulting in $\Delta = 27.4$ meV for 2 K $< T <$ 20 K and $\Delta = 223.1$ meV for 20 K $< T <$ 100 K.

Figure 2(a) shows the temperature-dependent resistivity $\rho(T)$ of RhP_2 single crystal. Clearly, RhP_2 has a semiconducting ground state. The behavior of $\log_{10}\rho$ versus $1/T$ is shown in Fig. 2(b). The $\rho(T)$ data can be fitted by the expression

$$\log_{10}\rho = A + 2.303\Delta/(k_B T), \quad (1)$$

where k_B is Boltzmann's constant, A is a constant, and Δ represents activation energy. The $\rho(T)$ data below 20 K and be-

tween 20 and 100 K were separately fitted by Eq. (1). An activation energy $\Delta_1 = 223.1$ meV was obtained by fitting, while the low-temperature range fit gives $\Delta_2 = 27.4$ meV, which is similar to the results previously reported for $FeSb_2$ (61 meV) and $RhSb_2$ (74 meV).[11,15] There was nearly no change in the magnetic-dependent resistivity $\rho(H)$ under 9 T and zero field, suggesting that magnetoresistance of RhP_2 single crystal is not sensitive to magnetic fields. We propose that the origin of the two transport band gaps is intrinsic in RhP_2. However, whether they are indirect gaps or not needs further evidence from optical conductivity or ARPES measurements. On the other hand, the impurity conduction as observed in many classical semiconductors cannot be excluded in this system. Perhaps in further experiments by isoelectronic chemical replacement slightly substituting As on the P site, we might manipulate the size of the two activated energy gaps.

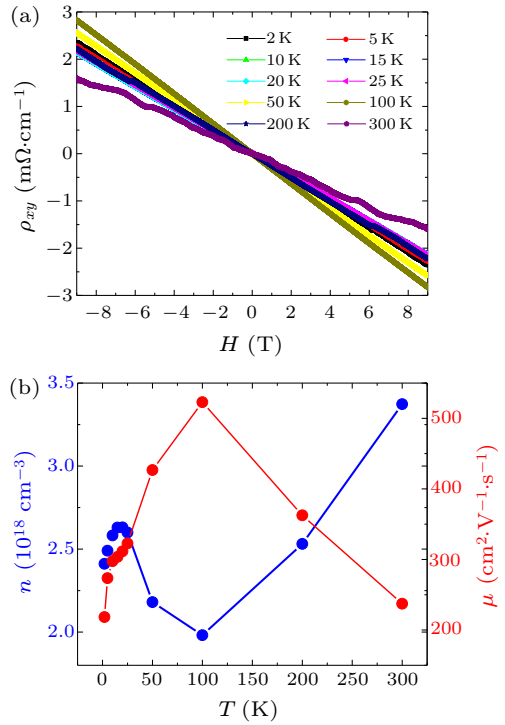


Fig. 3. Hall data, carrier densities, and mobilities of RhP_2. (a) Hall resistivity ρ_{xy} of RhP_2 single crystal at 2 K, 5 K, 10 K, 5 K, 20 K, 25 K, 50 K, 100 K, 200 K, and 300 K with applying field along [011] direction. (b) The carriers and mobilities results by fitting the Hall data using the single-band model.

Figure 3(a) present the Hall resistivity ρ_{xy} of RhP_2 with the magnetic field along the [011] direction and the electric current perpendicular to the [011] direction. From Fig. 3(a), the Hall resistivity data shows that the electron pocket dominates the transport behavior without sign changes. Using $R_H = -1/n_e$, the carrier density $n_e = 2.38 \times 10^{18}$ cm^{-3} at 2 K was obtained. We also obtained the effective electron mobility $\mu_e = 2.05 \times 10^2$ cm^2·V^{-1}·s^{-1}. Figure 3(b) shows the all-temperature dependence of n_e. The n_e increases with increasing temperature from 2 K to 25 K and reached a maximum of $n_e = 2.68 \times 10^{18}$ cm^{-3} at about 25 K. While with increasing temperature from 25 K to 100 K, the carrier density decreases to the minimum of $n_e = 2.0 \times 10^{18}$ cm^{-3} at 100 K. From 100 K to 300 K, the carrier density $n_e = 3.40 \times 10^{18}$ cm^{-3} with raising temperature. For charge carrier mobility $\mu_e = \sigma \times e \times n_e$, with the charge conductivity $\sigma(T) = 1/\rho(T)$. We obtained $\mu_e = 2.05 \times 10^2$ cm^2·V^{-1}·s^{-1} at 2 K increasing to its maximum at 100 K with $\mu_e = 5.45 \times 10^2$ cm^2·V^{-1}·s^{-1} at 100 K, then as temperature increases from 100 K to 300 K, μ_e decreases to 2.10×10^2 cm^2·V^{-1}·s^{-1} at 300 K. The charged center scattering or acoustic phonon scattering may play an important and competition role. Although two charge-carrier transport activated energy gaps exist, from the Hall plot we can only obtain almost linear magnetic dependent Hall results, which means that electron carriers from one electron pocket domain exhibit the transport behavior. The rapid increasing of μ_e with temperature in RhP_2 in the range 2 K–100 K reflects the dramatic decrease of the charge-carrier concentration. In the temperature range 100 K–300 K, we propose that the phonon scattering dominates the transport behaviors.

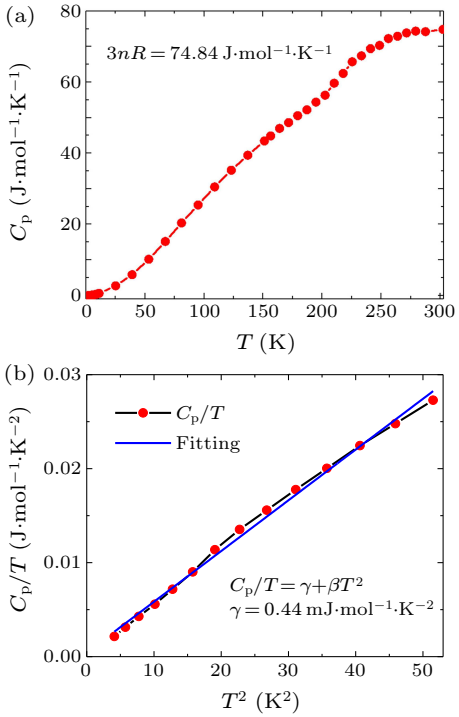


Fig. 4. (a) Temperate-dependent specific heat coefficient C_p for RhP_2. (b) Low-temperature specific heat fitting with formula $C_p/T = \beta T^2 + \gamma$ for RhP_2.

The heat capacity $C_p(T)$ decreases without showing any anomalies of RhP_2 in Fig. 4(a), suggesting no structural or magnetic transitions. The high-temperature heat capacity C_p(300 K) is approximately 74.84 J·mol^{-1}·K^{-1}, similar to the classical Dulong–Petit heat capacity $C_p = 3nR \approx$ 74.94 J·mol^{-1}·K^{-1}. The low-temperature specific heat in the form $C_p(T)/T$ vs. T^2 between 5 K and 2 K is shown in Fig. 4(b). The least-square analysis using the formula

$C_p(T)/T = \beta T^2 + \gamma$, where β is the lattice contributions to the $C_p(T)$ and γ represents the electronic contributions to the $C_p(T)$. We obtain $\gamma \approx 0.44$ mJ·mol^{-1}·K^{-2}. The nearly zero γ shows quite small density of states (DOS) at E_F, indicating typical semiconductor behavior of RhP_2, comparable to the bad metal behavior of $RhSb_2$.[15]

The temperature-dependent magnetic susceptibility $\chi(T)$ of RhP_2 displays diamagnetism from 5 K to 300 K. The value of $\chi(T)$ is almost temperature-independent. Here $\chi(T)$ at 2 K is only about 1×10^{-4} emu·mol^{-1}·Oe^{-1} under the magnetic field $H = 10$ K·Oe. Diamagnetic behavior is also confirmed by $\chi(H)$ data shown in Fig. 5(b).

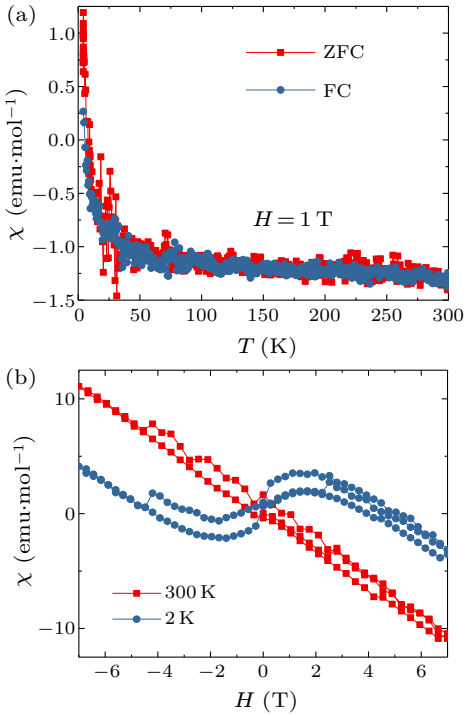


Fig. 5. (a) Zero field cooling (ZFC) and field cooling (FC) data of dc magnetic susceptibility measured of RhP_2. (b) The $\chi(H)$ data of RhP_2 at temperatures of 2 K and 300 K.

The physical properties of RhP_2 single crystals might be explained by the electronic band structure calculations. The band structure with the generalized gradient approximation (GGA) of Perdew–Burke–Ernzerhof method in Ref. [22] shows that with and without considering SOC, there is an energy band gap $\Delta = 0.755$ eV (without considering SOC) and $\Delta = 0.75$ eV (with considering SOC); in other two data bases,[23,24] the calculation results show that RhP_2 is topological trivial with a direct band gap $\Delta = 0.665$ eV or $\Delta = 0.3784$ eV.[23,24] The energy band gap Δ of RhP_2 is larger than the small gap reported for $RhSb_2$ at the Y_2 point of 0.074 eV.[15] In $RhSb_2$, some thermally activated carriers play an important role in transport properties. In RhP_2, the direct gap is one magnitude larger than that in $RhSb_2$, so it is difficult for thermally activated carriers to be sufficiently motivated above the Fermi level.

4. Conclusion

In conclusion, high-quality RhP_2 single crystal with an arsenopyrite-marcasite-type structure has been successfully synthesized by the Sn flux method. Single-crystal x-ray diffraction results shows that RhP_2 adopts a monoclinic structure with cell parameters of $a = 5.7347(10)$ Å, $b = 5.7804(11)$ Å, and $c = 5.8222(11)$ Å in space group $P2_1/c$ (No. 14). RhP_2 exhibits a narrow-bandgap semiconductor behavior with the activation energies of 223.1 meV and 27.4 meV for two distinct regions, respectively, from the temperature-dependent electrical resistivity $\rho(T)$ measurements. By single-band model fitting, we obtain carrier concentrations of $n_e = 2.38 \times 10^{18}$ cm^{-3} at 2 K from the Hall coefficient using $R_H = -1/n_e$. For charge carrier mobility, $\mu_e = 2.05 \times 10^2$ cm^2·V^{-1}·s^{-1} at 2 K, increasing to its maximum at 100 K with $\mu_e = 5.45 \times 10^2$ cm^2·V^{-1}·s^{-1}, then with temperature further increasing from 100 K to 300 K, $\mu_e = 2.10 \times 10^2$ cm^2·V^{-1}·s^{-1} at 300 K. By fitting the low temperature heat capacity data with $C_p/T = \gamma + \beta T^2$, the electronic specific heat coefficient $\gamma = 0.44$ mJ·mol^{-1}·K^{-2}. Further optimizations of carrier density, band structures, pressure effect, and doping level will be helpful for realizing superconductivity and novel topological quantum states. Our results not only offer a useful platform for platform for studying exotic physical properties and electron band structures, but also motivate further exploration of their potential photovoltaic and optoelectronic applications.

Acknowledgments

We are grateful to Professor Y. T. Song (Institute of Physics, CAS) for his assistance in the x-ray diffraction experiments. This work was supported by the National Key Research and Development Program of China (Grant No. 2017YFA0302901), the Strategic Priority Research Program, the Key Research Program of Frontier Sciences of the Chinese Academy of Sciences (Grant No. XDB33010100), the National Natural Science Foundation of China (Grant Nos. 12134018, 11921004, and 11634015), the Foundation of Quantum Science Center of Guangdong–Hong Kong–Macao Greater Bay Area, China (Grant No. QD2301005), the Postdoctoral Science Foundation of China (Grant No. 2021M693370), and the Synergetic Extreme Condition User Facility (SECUF).

References

[1] Cheng P and Yang Y 2022 *Acc. Chem. Res.* **53** 1218
[2] Sitt A, Hadar I and Banin U 2013 *Nano Today* **8** 494
[3] An S, Park H J and Kim M 2023 *J. Mater. Chem. C* **11** 2430
[4] Baker I M 2017 2017 *Springer Handbook of Electronic and Photonic Materials* (Berlin: Springer) p. 1

[5] Massidda S, Continenza A, Freeman A, Freeman J, de Pascale T M, Meloni F and Serra M 1990 *Phys. Rev. B* **41** 12079

[6] Klimov A E and Shumsky V N 2009 *Physica B* **404** 5028

[7] Castellanos-Gomez A 2015 *J. Phys. Chem. Lett.* **6** 4280

[8] Prytz Ø and Flage Larsen E 2009 *J. Phys.: Condens. Matter* **22** 015502

[9] Zhang S, Ou X, Xiang Q, Carabineiro Sónia A C, Fan J and Lv K 2022 *Chemosphere* **303** 135085

[10] Niu S, Huyan H, Liu Y, Yang L, Yeung M, Ye K, Blankemeier L, Orvis T, Sarkar D, Singh D J, Kapadia R and Ravichandran J 2017 *Adv. Mater.* **29** 1604733

[11] Johnston W D, Miller R C and D H Damon 1965 *J. Less-Common Met.* **8** 272

[12] Hulliger F 1964 *Nature* **201** 381

[13] Fjellvåg H, Selte K and Stave F E 1984 *Acta Chem. Scand. A* **38** 687

[14] Sun P, Oeschler N, Johnsen S, Iversen B and Steglich F 2009 *Phys. Rev. B* **79** 153308

[15] Wu D S, Qian Y T, Liu Z Y, Wu W, Li Y J, Na S H, Shao Y T, Zheng P, Li G, Cheng J G, Weng H M and Luo J L 2020 *Chin. Phys. B* **29** 037101

[16] Lee K, Lange G. F, Wang L L, Kuthanazhi B, Trevisan T V, Jo N H, Schrunk B, Orth P P, Slager R, Canfield P C and Kaminski A 2021 *Nat. Commun.* **12** 1855

[17] Hulliger F 1963 *Phys. Lett.* **4** 282

[18] Kjekshus A, Nolander B, Klaeboe P, Cyvin S J, Lagerlund I and Ehrenberg L 1971 *Acta Chem. Scand.* **25** 411

[19] Goodenough J B 1972 *J Solid State Chem.* **5** 144

[20] Wu D S, Mi Z Y, Li Y J, Wu W, Li P L, Song Y T, Liu G T, Li G and Luo J L 2019 *Chin. Phys. Lett.* **36** 077102

[21] http://shelx.uni-goettingen.de/

[22] Topological properties and more for material P_2Rh (sg14) — Materiae (iphy.ac.cn)

[23] Topological Materials Database (topologicalquantumchemistry.org)

[24] https://atomly.net/#/matdatades/0000084348